# Fluctuations in Calorimetry Measurements

Physica Scripta, Vol. 23, 409–424, 1981

# Fluctuations in Calorimetry Measurements

Ugo Amaldi

CERN, CH 1211 Geneva, Switzerland

*Received November 13, 1980; accepted November 14, 1980*

**Abstract**

Calorimeters are used in high energy physics to measure energy, position, direction and sometimes nature of a primary particle. Their properties are reviewed here with particular emphasis on the qualitative understanding of the relations between the physics of the cascade processes and the performances of actual instruments. The accent is put on energy measurements of photons and hadrons, but the limits achieved in determining the spatial position of electromagnetic and hadronic showers are also presented and discussed.

## 1. Introduction

In high energy physics calorimeters are blocks of matter in which the energy of a particle is degraded to the level of detectable atomic ionizations and excitations. They are used to measure not only the energy, but also the spatial position, the direction and, in some cases, the nature of the primary particle. Their performances, which improve with increasing energy, are limited both by the unavoidable fluctuations of the elementary phenomena through which the energy is degraded and by the technique chosen to measure the final products of the cascade processes. This paper sketches the status of the present knowledge of these two classes of limiting factors by treating electromagnetic showers (Section 2) and hadronic showers (Section 3). In Sections 2 and 3 energy and position measurements are discussed one after the other, but a larger emphasis is given to the discussion of energy fluctuations. Section 4 is devoted to the description of some techniques recently introduced to reduce the effect of different types of fluctuations and aims at stimulating new ideas.

It has to be stressed that, although we have a clear understanding of the elementary degradation processes, in most cases a gap exists between general cascade theories and the explanation of the experimental findings. In many instances Monte Carlo calculations fill the gap, however, the presentation of the subject is by necessity phenomenological and the selection of the basic data among the large variety of available results becomes a matter of personal choice. Further references can be found in the Proceedings of the Fermilab Workshop [1] and in the recent review article by Seigi Iwata [2].

## 2. Electromagnetic showers

### 2.1. *General properties*

The longitudinal development of an electromagnetic shower in matter is determined by the radiation length $X_0$. The lateral spread of a shower is mainly due to the multiple scattering of the electrons that do not radiate but have a large enough energy to travel far away from the axis. The energy of an electron that loses as much energy in collisions as in radiation has the name of critical energy $\epsilon$, so that the natural transverse unit of a shower is the lateral spread of an electron beam of energy $\epsilon$ after traversing a thickness $X_0$:

$$R_M = \frac{E_s}{\epsilon} X_0, \quad (E_s = 21\ \text{MeV}) \tag{1}$$

$E_s$ is the usual constant appearing in multiple scattering theory [3]. The formulae giving the radiation unit $X_0$ and the Molière unit $R_M$ are rather complicated. For rapid estimates one can use the approximate expressions

$$\begin{aligned} X_0 &\simeq 180 \frac{A}{Z^2} \frac{\text{g}}{\text{cm}^2} \left( \frac{\Delta X_0}{X_0} < \pm 20\% \text{ for } 13 \leqslant Z \leqslant 92 \right) \\ \epsilon &\simeq \frac{550}{Z}\ \text{MeV} \quad \left( \frac{\Delta \epsilon}{\epsilon} < \pm 10\% \text{ for } 13 \leqslant Z \leqslant 92 \right) \\ R_M &\simeq 7 \frac{A}{Z} \frac{\text{g}}{\text{cm}^2} \quad \left( \frac{\Delta R_M}{R_M} < \pm 10\% \text{ for } 13 \leqslant Z \leqslant 92 \right) \end{aligned} \tag{2}$$

We remark that the ratio $\epsilon/X_0$ equals the minimum collision loss, which in the above approximation is simply

$$\left( \frac{\Delta E}{\Delta x} \right)_{\text{min}} = \frac{\epsilon}{X_0} \simeq 3 \frac{Z}{A} \frac{\text{MeV cm}^2}{\text{g}} \tag{3}$$

The quantity which is usually introduced to represent the spatial development of the shower is the differential distribution of the "track length" $T$, defined as the sum of the tracks of all the charged particles of the shower. The quantity $T$ depends upon the cut-off energy $E_c$, the minimum kinetic energy of an electron (positron) that can be detected in the calorimeter. For $E_c = 0$ all the electrons and positrons are detected and the total track length $T/X_0$ expressed in $X_0$ units is equal to $E/\epsilon$. For increasing values of the cut-off energy the fractional useful track length $F$ decreases as shown in Fig. 1, where we have plotted vs. $E_c/\epsilon$ results of calculations performed in various materials. The dashed line represents the result of an analytic calculation performed by Tamm and Belenky by using what is called "Approximation B" by Rossi [3]. In this approximation (a) all electrons lose a constant amount of energy $\epsilon$ per radiation length $X_0$ and (b) radiation phenomena and pair production at all energies are described by the asymptotic formulae for large energies. In this approximation the results are identical for all substances, provided one measures the thickness in $X_0$ units and energies in $\epsilon$ units. The dashed line represents the result of such a calculation for $E \gg E_c$ ($z = 2.29\, E_c/\epsilon$)

$$F(z) = 1 + z\, e^z Ei(-z) \simeq e^z \left[ 1 + z \ln \left( \frac{z}{1.526} \right) \right] \tag{4}$$

The last equation is valid within 10% for $z \leqslant 0.3$. The dotted curves of Fig. 1 represent numerical computations in lead and air by Richards and Nordheim, who assumed a continuous energy loss for the electrons [3], and indicate the difference between light and heavy materials. As expected, Approxi-

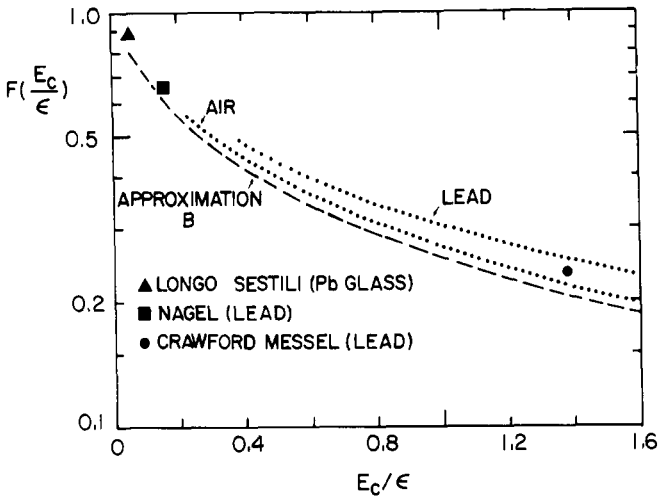


*Fig. 1.* Compilation of results concerning the fraction $F$ of the total track length which is seen on average in a fully contained electromagnetic shower. The dotted lines represent the numerical calculations by Richards and Nordheim [3] and the points represent Monte Carlo results [4–6].

mation B (dashed line) is valid for *light* materials. Finally, the solid points give the results of various Monte Carlo calculations. We find that the data for different materials can be put on an almost universal curve by redefining the variable $z$ in eq. (4):

$$z = 4.58 \frac{Z}{A} \frac{E_c}{\epsilon} \tag{5}$$

In summary the track length can be written with a good approximation as

$$T = F(z) \frac{E}{\epsilon} X_0 \tag{6}$$

and calorimetry is possible because, for any given value of $E_c$, the total track length is proportional to the energy $E$.

The distribution of the longitudinal track length, which is proportional to the longitudinal energy deposition, is well represented by the formula [6]:

$$\frac{dE}{dt} = E_0 \frac{b^{\alpha+1}}{\Gamma(\alpha+1)} t^{\alpha} e^{-bt}, \quad \left(t = \frac{x}{X_0}\right) \tag{7}$$

The parameters $\alpha$ and $b$ are energy dependent and have been computed by Longo and Sestili for photon showers of less than 5 GeV in lead glass [6]. $b$ is of the order of 0.5 and $\alpha$ is related to it through the position of the shower maximum $t_{max} = \alpha/b$ [7]. The median depth of the shower, i.e., the depth at which half of the incident energy is deposited, is given by the expression:

$$t_{med} = \left[\ln\left(\frac{E}{\epsilon}\right) + a\right] \quad (a = 0.4 \text{ or } 1.2 \text{ for } e\text{'s or } \gamma\text{'s}) \tag{8}$$

The median depth is related to the maximum of the shower $t_{max} \simeq t_{med} - 1.5$.

The knowledge of the longitudinal distribution of the shower allows us to compute the calorimeter length $L(98\%)$ needed to contain a fixed fraction of the incident energy. It turns out that

$$L(98\%) \simeq 3 t_{med} \tag{9}$$

where $t_{med}$ is given by eq. (8).

Equation (7) represents the *average* longitudinal distribution

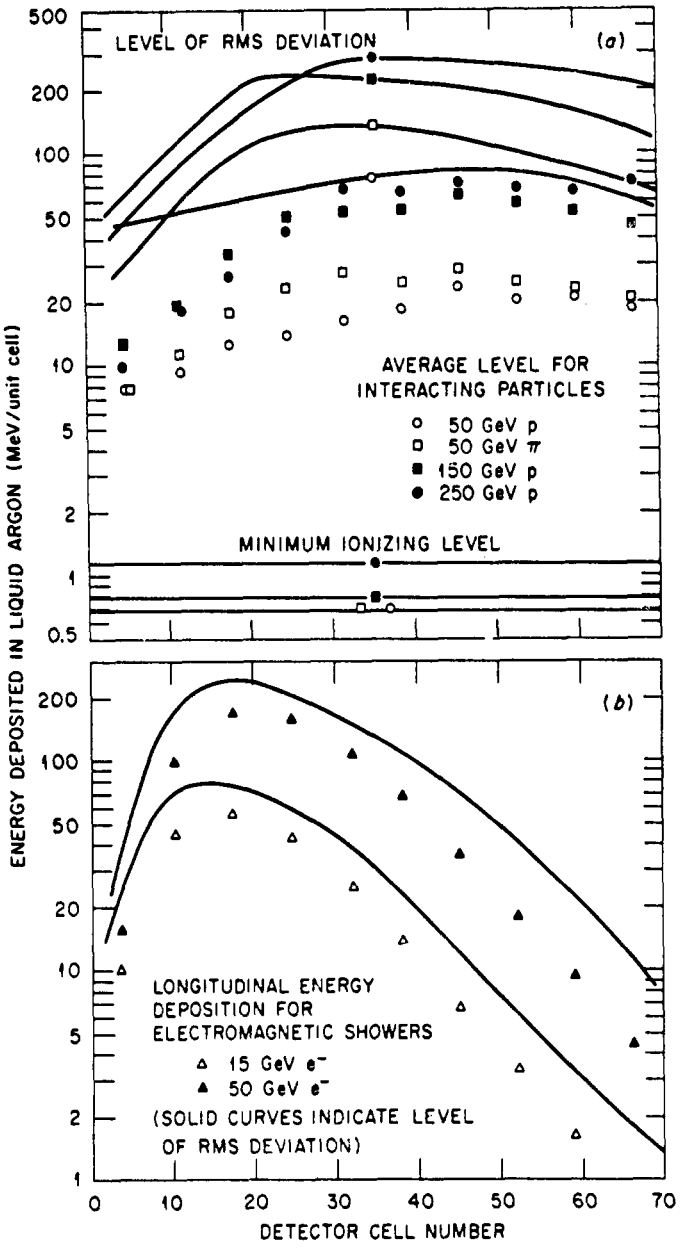


*Fig. 2.* Average longitudinal distribution of hadronic (a) and electromagnetic (b) showers in a lead–liquid argon calorimeter as computed by Jensen et al. [8]. The cell is made of 2 mm Pb and 1 mm of liquid argon for a total depth of 27 radiation lengths. The solid curves indicate the r.m.s. deviations from the mean values.

of a shower. For energy measurements even more important are the fluctuations in the shower development due to the statistical nature of the cascade processes. The r.m.s. values of the fluctuations for electromagnetic showers in liquid argon are given in Fig. 2(b) computed with a Monte Carlo program by Jensen, Amburgey and Gabriel [8]. Typically the fluctuations multiply or divide the average deposited energy by a factor 1.5. This factor does not contain enough information, because the energies deposited at different depths are strongly correlated. Figure 3 shows the correlations observed by Cerri and Sergiampetri in the energy deposited longitudinally in an argon calorimeter [9]. As expected, positive fluctuations in the region before the maximum of the shower correspond to negative ones on the tail and vice versa.

It has been stated above that the transverse development of a shower is governed by the Molière length $R_M$. This is not exactly true because, as shown in Fig. 4 (adapted from [10]), two dif-

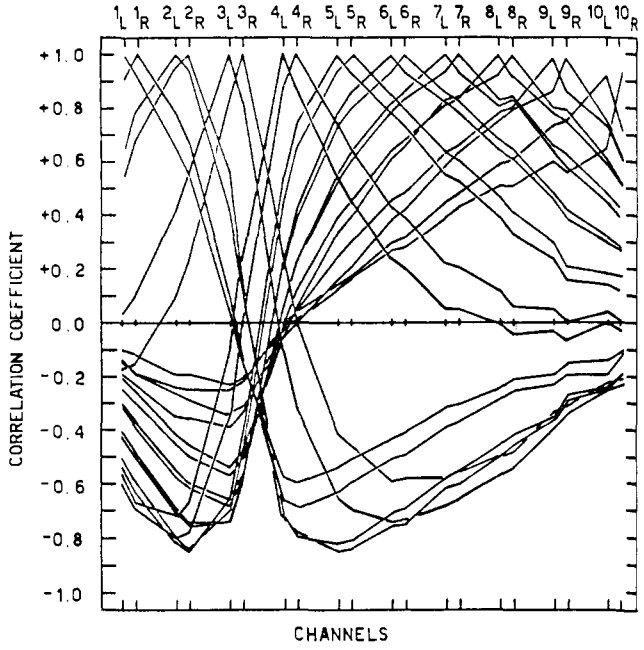


*Fig. 3.* Correlation coefficients between the energy deposited in the cells of an iron–liquid argon calorimeter. The measurements by Cerri and Sergiampietri [9] were made on a calorimeter with 400 layers each 1 mm iron + 1 mm argon thick. The layers were assembled in 20 cells of 1.3 radiation length. The measurement was performed with 25 GeV electrons.

ferent mechanisms contribute to the transverse distribution. The central part scales as $R_M$ and is due to multiple scattering effects, while the peripheral part is mainly due to the propagation of the photons that are less attenuated in matter (10–20 MeV in lead). The spatial distribution of this component is determined by the minimum value of the photon attenuation coefficient, which has no simple dependence upon $A$ and $Z$ [11]. Still, 95% of the total energy is contained in a cylinder having the radius

$$R(95\%) \simeq 2R_M \simeq 14 \frac{A}{Z} \frac{\text{g}}{\text{cm}^2} \qquad (10)$$

## 2.2. *Effect of containment on energy resolution*

The intrinsic energy resolution of an active calorimeter of infinite dimensions is limited by the statistics of the elementary processes and was computed to be [6]

$$\frac{\sigma(E)}{E} = \frac{\sigma(T)}{T} \simeq \frac{0.7\%}{\sqrt{E(\text{GeV})}}; \quad (E_c/\epsilon = 0.5/11.8 = 0.04) \qquad (11)$$

This result applies to fully contained showers. Any lack of containment spoils the resolution. As a consequence not only the energy measurement is worsened but also the distribution of the output signals observed for monochromatic electrons acquires a tail extending towards zero. In the following this last effect will be neglected because we shall consider mainly small leakage losses.

The marble fine grained calorimeter of the CHARM Collaboration [12] has been used to determine the effect of longitudinal and lateral losses in a low-$Z$ material ($\langle Z \rangle \simeq 13$). Figure 5 shows that the longitudinal losses are much more dangerous than the lateral ones. A 5% lateral loss spoils the energy resolution much less than a 2% longitudinal loss. Eqs. (9) and (10) give the rough calorimeter dimensions which correspond to such a containment. They are valid for energies of the order of 10 GeV. Prokoshkin [13] has extrapolated them up to 100 TeV and finds that at 100 GeV $L(98\%) \simeq 2.6t_{max}$ and at 1 TeV $L(98\%) \simeq 2.4t_{max}$. For showers in lead glasses the same paper gives for the degraded resolution the formula:

$$\text{lead glass:} \quad \frac{\sigma(E)}{E} \simeq \left[\frac{\sigma(E)}{E}\right]_{L=\infty} (1 + 4f + 50f^2) \quad (f < 0.1) \qquad (12)$$

where $f$ is the fractional energy loss.

For a calorimeter of fixed dimensions, the fraction of the energy lost longitudinally increases with energy. Measurements in lead and iron of the resolution due to leakage fluctuations can be fit by an exponential form, $A \exp(-L/\zeta)$, where $L$ is the calorimeter length and $A$ and $\zeta$ depend weakly on incident energy [23]. For a fixed length the overall energy dependence of the resolution due to leakage is also weak, but does not follow any simple law.

## 2.3. *Homogeneous calorimeters*

We now pass to consider fully active calorimeters, typically homogeneous calorimeters in which the degraded energy is measured by collecting visible photons. The energy resolution of the best performing one, sodium iodide, is limited by leakage fluctuations. Indeed the resolution of a 24 radiation length long NaI crystal follows the law $\sigma(E)/E \simeq 0.9\%/E^{1/4}$ ($E$ in

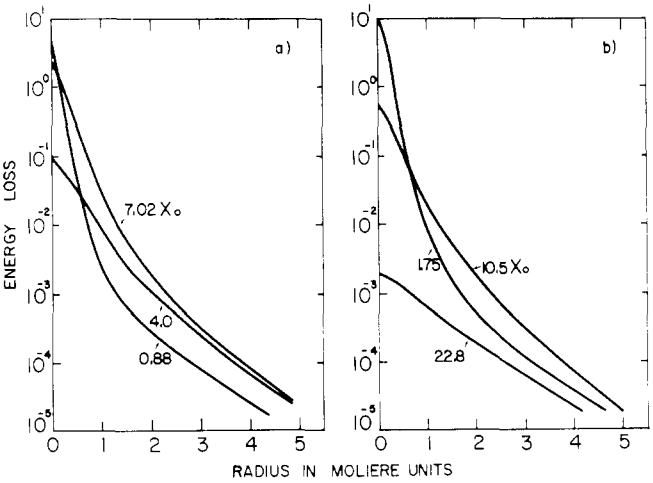


*Fig. 4.* Monte Carlo calculations by Yuda [10] on the lateral distribution of energy deposited by a 1 GeV shower in lead. Note the two different components, particularly visible at small depths.

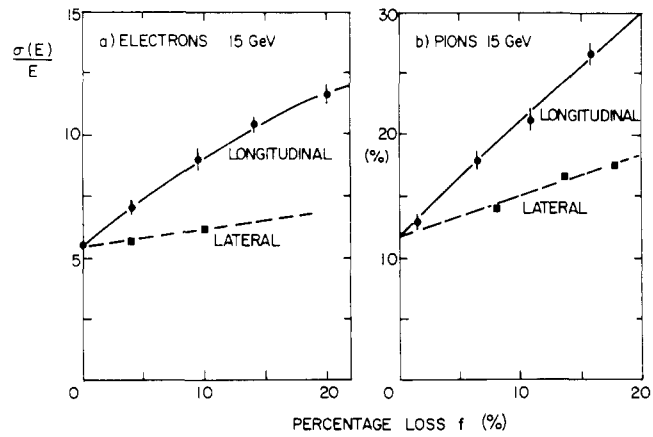


*Fig. 5.* Effect of the longitudinal and lateral losses on the energy resolution as measured for electrons (a) and for pions (b) by the CHARM Collaboration in a low-$Z$ calorimeter.

GeV) [14]. The peculiar energy dependence and the fact that at 1 GeV this resolution is close to the intrinsic limit of eq. (8), while at 10 GeV it is larger by about a factor of two, indicate that the limiting factor is neither the cascade process nor the statistics of the photoelectrons (which would also give an $E^{-1/2}$ law). At variance with the case of NaI, the resolution obtainable with lead-glass counters is mainly limited by photon statistics. Typically $g = 1000$ photoelectrons are produced per GeV and, for fully contained showers, the resolution takes the form [13]

$$\left[\frac{\sigma(E)}{E}\right]_{L=\infty} = \left[\frac{\sigma_0^2(E)}{E^2} + \frac{1}{\xi g E}\right]^{1/2} \simeq 0.006 + \frac{0.03}{\xi^{1/2} E^{1/2}} \qquad (13)$$

where $\xi$ is the ratio of the photocathode area to that of the radiator exit (typically $\xi \leqslant 0.5$) and $\sigma_0(E)$ is an energy dependent contribution which is due not only to shower fluctuations (eq. (8)) but also to the absorption of the Cerenkov light in the radiator itself. In Section 4 we shall come back to the use of light filters to reduce these types of fluctuations.

### 2.4. *Sampling fluctuations*

In a sampling calorimeter the degraded energy is measured in a number of sensitive layers interspersed by passive absorber. In this case the intrinsic resolution of eq. (11) is always negligible and the leakage contributions can be treated as done above in Section 2.2.

The dominating causes of fluctuations have to be discussed separately for two different classes of calorimeters: *digital* and *proportional* ones. In digital devices the fluctuations are dominated by "sampling fluctuations". These are the fluctuations in the total number of electron and positron tracks crossing the sensitive planes. In proportional calorimeters other effects have to be taken into account, as will be made clear in the following.

Let us first consider the fluctuations of the number of crossings $N$. For $E_c = 0$ the total track length $T$ in a shower is given by eq. (6): $T = EX_0/\epsilon$. In Approximation B the shower has $n$ lateral spread and in an infinitely long medium a set of planes equally spaced at distance $x$ intercepts a number of tracks equal to the ratio $T/x$ independently of the longitudinal distribution of the electrons and the positrons

$$N = \frac{E}{\epsilon}\frac{X_0}{x} = \frac{E}{\delta E} \qquad (14)$$

The last relation follows from the fact that $\epsilon/X_0$ equals the minimum energy loss (eq. (3)); $\delta E$ is then the energy lost by a minimum ionizing particle in traversing one layer of thickness $x$.

By counting the number of crossings $N$ and by assuming that the crossings are independent and their number follows a normal distribution, one can measure the energy with an r.m.s. error which is due only to sampling fluctuations:

$$\left(\frac{\sigma(E)}{E}\right)_{\text{SAMPLING}} \simeq \frac{1}{\sqrt{N}} = \sqrt{\frac{\delta E}{F(z)E}} = 3.2\%\sqrt{\frac{\epsilon(\text{MeV})}{F(z)}} \times \sqrt{\frac{t}{E(\text{GeV})}} \qquad (15)$$

The factor $F(z)$, defined in eqs. (4) and (5), takes into account the shortening of the track length due to the cut-off energy $E_c$. As usual $t = x/X_0$ is the thickness of a calorimeter layer expressed in radiation lengths. To obtain a resolution as good as in a lead glass Cerenkov (eq. (13)) one must have $\epsilon t \simeq 1$, i.e., a

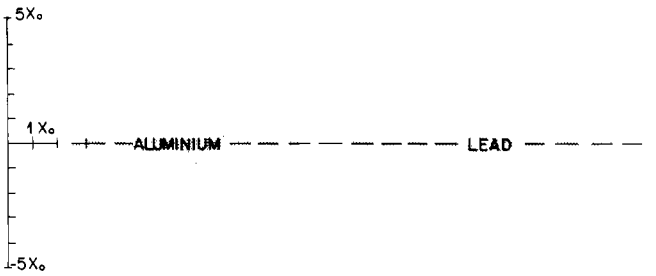


*Fig. 6.* Schematic representation of the cross-section of the volume that contains, on average, about 90% of the total energy of an electromagnetic shower. The units are radiation lengths on both axes.

glass Cerenkov counter is equivalent to a sampling calorimeter whose layers have thickness $t \simeq 1/\epsilon$ (MeV), i.e., $x \simeq 0.15X_0$ in lead. It has to be stressed that for very small values of $t$ one does not expect that the low $t^{-1/2}$ continues to apply due to the correlations between the number of crossings detected in successive sensitive planes.

Equation (15) follows from Approximation B and applies to the counting of the total number of shower tracks traversing the sensitive plane immersed in a light material. In Fig. 6 we compare the spatial distributions of an electromagnetic shower in a low-$Z$ and in a high-$Z$ material: the transverse dimensions, measured in radiation lengths, are much larger in lead than in aluminium, because the Molière length scales as $R_M/X_0 = E_s/\epsilon$ (eq. (1)). Thus in a heavy material the electrons and the positrons form larger angles with respect to the shower axis than in a light one, and this effect is not considered in Approximation B. Figure 7 is taken from Fisher's Monte Carlo calculation [15] and shows that in lead a sizeable fraction of the low energy electrons form large angles $\theta$ with respect to the shower axis. To qualitatively understand the $Z$-dependence of this effect we have constructed a simplified model that divides all electrons which cross the active planes in two categories: (i) electrons that have $\theta = 0$ and energy $e_0 \leqslant e$ and (ii) electrons that are uniformly distributed and have energy $0 \leqslant e \leqslant e_0$. Figure 7 shows that in lead one should take $e_0 \simeq 4$ MeV, i.e., $e_0/\epsilon \simeq 1/2$. The simple model, supplemented with this input

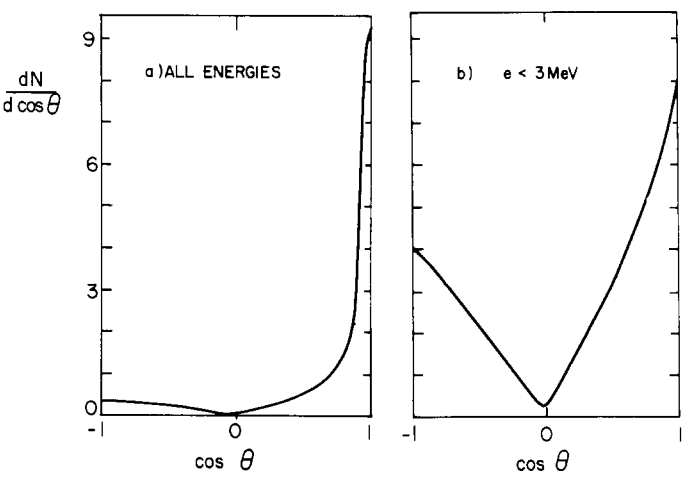


*Fig. 7.* Angular distributions of the electrons moving in the gaps of a lead quantameter with 48 samples for a total depth of $16X_0$ ($t = 1/3, E = 1$ GeV) [15]. The electrons are cut at energies $e < 1$ MeV. Numerical calculations indicate that the "isotropic" low energy component should have a distribution proportional to $\cos^2\theta$. The Monte Carlo by Fisher suggests a distribution $\sim |\cos\theta|$. According to this calculation $\sim 12\%$ of all the electrons move backwards in the gaps.

from the Monte Carlo, allows the calculation of the fraction $\alpha$ of all the $N$ crossings that belong to category (ii).

$$\alpha \simeq \frac{1}{2}\left(\frac{E_s}{\pi\epsilon}\right)^2; \quad (E_s = 21\,\text{MeV}; E_c = 1\,\text{MeV}) \tag{16}$$

This equation shows that the number of large angle electrons decreases as $\epsilon^2$, being large (of the order of 40%) in lead and small ($< 2\%$) in aluminium. Of course, $\alpha$ decreases when the cut-off energy $E_c$ increases. Figure 8 shows how the fraction $\alpha$ depends upon $E_c$ in our simple minded model. With active plates of thickness $x_a$, it is reasonable to assume that $E_c \simeq (x_a/2)(\Delta E/\Delta x)$, as indicated by the upper scale of Fig. 8. The curves then show in a *qualitative* way why dense active planes thicker than 1 g cm$^{-2}$ are insensitive to the large angle electrons, while gas detectors with $d = 10^{-3}$–$10^{-2}$ g cm$^{-2}$ are expected to be severely affected by their presence. The figure also shows that in iron, and even more in aluminium, this phenomenon is much less important.

Let us now consider its effect on the sampling resolution, which for light material is given by eq. (15). To a track forming an angle $\theta$ with the shower axis, the sensitive layers appear at an effective distance $t/\cos\theta$, so that eq. (15) has to be corrected by an average factor $\langle\cos\theta\rangle^{-1/2}$. The angle $\theta$ must depend on $R_M/X_0$, i.e., on $E_s/\epsilon$, but only a comparison with a Monte Carlo calculation can suggest a quantitative relation. As above, we use the calculation by Fisher [15] ($t = 1/3, E_c = 1$ MeV) to obtain, by comparing with eq. (15), the expression

$$\langle\cos\theta\rangle \simeq \cos\left(\frac{E_s}{\pi\epsilon}\right); \quad (E_s = 21\,\text{MeV}) \tag{17}$$

This expression is valid when the cut-off energy is not too large and from our simple model we infer that the condition is $E_c\,(\text{MeV}) \leqslant 10/\epsilon\,(\text{MeV})$. The sampling resolution then becomes (with $F(z)$ defined in eq. (4))

$$\left(\frac{\sigma(E)}{E}\right)_{\text{SAMPLING}} = 3.2\%\sqrt{\frac{\epsilon\,(\text{MeV})}{F(z)\cos(E_s/\pi\epsilon)}}\sqrt{\frac{t}{E\,(\text{GeV})}}$$

$$= 3.2\%\sqrt{\frac{\delta E\,(\text{MeV})}{F(z)\cos(E_s/\pi\epsilon)}}\sqrt{\frac{1}{E\,(\text{GeV})}} \tag{18}$$

This equation gives for $t = 1/3$ and $z = 0$ in lead $\sigma(E)/E \simeq 6.5\%$, as computed by Fisher and, with a cut $E_c = 1.0$ MeV, corresponds to a number of tracks in lead $N \simeq 55E\,(\text{GeV})/t$, in good agreement with the Monte Carlo results by Nagel [4] who found $N \simeq 50E\,(\text{GeV})/t$.

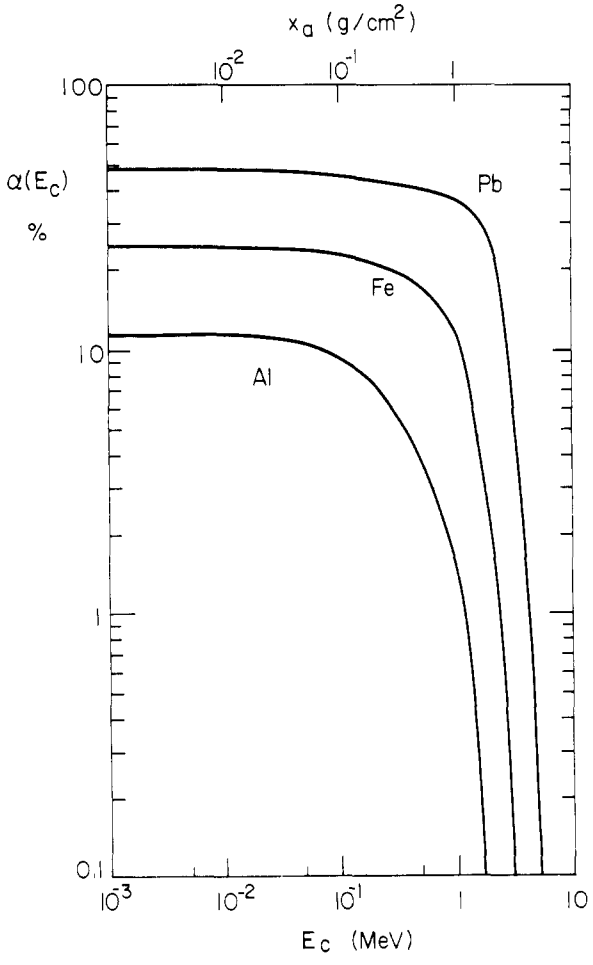


*Fig. 8.* By $\alpha$ we indicate the fraction of all the electrons and positrons traversing the gaps which belong to the "isotropic" component. The sampled fraction decreases with the cut-off energy $E_c$, i.e., with the thickness $x_a$ of the active layers. The curves are the prediction of a very simple model and are only meant to show two features of the phenomenon: (i) the effect decreases drastically with $Z$; (ii) in low-$Z$ quantameters one can have smaller cut-off energies and still achieve the same percentage reduction of the effect.

Our formula for the sampling fluctuations deserves three remarks. First, to grasp the origin of the observed resolutions we have corrected the simple estimate of eq. (14) obtained in Approximation B by taking into account the cut-off energy $E_c$ and the scattering of low energy electrons. In the factor $[F\langle\cos\theta\rangle]^{-1/2}$ we have lumped other less important effects neglected in Approximation B, in particular the fact that in a high-$Z$ material the assumption of a constant absorption of gammas is incorrect even for energies larger than $\epsilon$, so that there are more low energy photons and electrons than predicted by Approximation B. Second, it has to be remarked that the fact that eq. (14) overestimates the number of tracks in lead was noted a long time ago. Willis and Radeka [16] attributed the discrepancy to the fact that electrons and positrons are always created in pairs, so that the number of statistically independent crossings is $N/2$ and not $N$. We believe that this cannot be the main contribution to the widening of the resolution in lead because the argument would hold for light materials too and, for instance, it would predict a much too poor resolution for the marble calorimeter of the CHARM Collaboration: $\sigma(E)/E \simeq 28\%/E^{1/2}$ instead of the measured value $20\%/E^{1/2}$. The last remark has to do with the dependence upon the cut-off energy $E_c$ of the two correcting factors $F(z)$ and $\cos(E_s/\pi\epsilon)$. With increasing $E_c$ the first factor decreases while the second one increases, because the isotropic component of the shower is less sampled, as qualitatively shown in Fig. 8. We can thus expect a rough compensation between the two corrections and a wide range of validity for eq. (18).

Sampling fluctuations domine the resolution of *digital calorimeters*. The "flash calorimeter" based on the use of Conversi tubes [17] is the best known of them. In the most recent versions the sensitive planes are made of extruded plates of polypropylene forming tubular cells of 3.5 x 5 mm$^2$ transverse dimensions [18]. The measured resolution for a calorimeter with lead plates of thickness $t = 0.9$ is $\sigma(E)/E \simeq 12\%/E^{1/2}$ (GeV), in the energy range 0.5–3 GeV, in good agreement with eq. 18 which gives $11\%/E^{1/2}$ (GeV) for $E_c \simeq 0$. The response of the calorimeter is non-linear above $\sim 3$ GeV, because the density of

the tracks increases and there is more than one crossing per cell. For the chosen cell size this limits the achievable resolution at energies larger than 5 GeV to $\simeq 6\%$. Recently a multiwire detector consisting of an array of cubic cells operated in the limited streamer mode has been proposed as a new fast digital calorimeter whose resolution would be limited by sampling fluctuations [19].

### 2.5. *Landau and path length fluctuations*

The sensitive material in a proportional calorimeter has either high density (solid or liquid) or low density (gas). In both cases other sources of fluctuations have to be considered. They dominate the behaviour of gas proportional calorimeters (multiwire quantameters) while contributing minor corrections to the sampling fluctuations in the case of solid or liquid detectors. One usually distinguishes two different contributions to the resolution: *Landau fluctuations* and *path length fluctuations*.

Minimum ionizing particles traversing a thickness $x$ of material give an asymmetric distribution of deposited energy $e$ whose r.m.s. value has the form [20]

$$\frac{\sigma(e)}{e} \simeq \frac{2}{\ln(4W/E_m)} \tag{19}$$

where $W$ is the energy above which on the average one $\delta$ ray is produced in the thickness $x$:

$$W(\text{MeV}) = 0.15 \frac{Z}{A} x(\text{g cm}^{-2})] \tag{20}$$

and $E_m$ is the minimum energy of a $\delta$-ray, usually taken to be of the order of 30 eV. The tail of the Landau distribution is such that the contribution to the total energy resolution of $N$ crossings is not quite proportional to $N^{-1/2}$, but for an order of magnitude estimate one can still combine eq. (19) and eq. (20) and write

$$\left(\frac{\sigma(E)}{E}\right)_{\text{LANDAU}} \simeq \frac{1}{\sqrt{N}} \frac{2}{\ln[10^4 x(\text{g cm}^{-2})]} \tag{21}$$

For a detector thickness $x = 1\,\text{g cm}^{-2}$ this increases the sampling fluctuation by less than 3%. In a gas quantameter $x \simeq 10^{-3}\,\text{g cm}^{-2}$ and eq. (21) would predict a widening of the sampling resolution by a factor $\sim\sqrt{2}$. The actual situation is worse than this [20] since Landau formula underestimates the pulse height distribution in a gas by about a factor of two because it neglects electron binding [21, 22].

The wide spread of electron angles discussed above corresponds to large fluctuations in the path length that the electrons themselves make in the active material of the calorimeter. These path length fluctuations are much larger in a gas than in a solid active material for two reasons: (i) the cut-off energy is much smaller in gas and low energy electrons that move along a sensitive layer leave much more energy than electrons which move perpendicularly to the plane; (ii) in a dense layer multiple scattering is much larger than in gas, so that the electrons tend to be scattered out of the dense layer with a corresponding reduction of the path length and of its fluctuations.

In summary Landau and path length fluctuations give small contributions in a calorimeter with dense proportional layers, and the sampling fluctuations are expected to dominate, as confirmed by the comparison reported in Table I, where we list computed and measured values for the quantity $R$ defined through the relation:

$$\frac{\sigma(E)}{E} = R(\%) \sqrt{\frac{t}{E(\text{GeV})}} \tag{22}$$

For iron and lead we have taken an experiment in which the data have been carefully corrected for leakage fluctuations and photoelectron statistics [23]. The "aluminium" point was obtained by the CHARM collaboration with a very large marble calorimeter equipped with thick scintillators (marble and aluminium have practically identical properties). By comparing the measured with the computed $R$-values we conclude that eq. (18) gives a good representation of the data [24]. Of course, it cannot substitute accurate measurements or detailed Monte Carlo calculations, but it has the advantage of showing in a transparent way the main corrections that have to be applied to the formula derived in Approximation B. It is worth remarking that our equation 18 for the sampling fluctuations differs greatly from the one proposed by Iwata, as shown in the last column of Table I, whose entries were computed with the formula [2]:

$$\left(\frac{\sigma(E)}{E}\right)_{\text{SAMPLING}} \simeq 2.0 \sqrt{e(\text{MeV}) X_0(\text{g cm}^{-2})} \sqrt{\frac{t}{E(\text{GeV})}}\,\% \tag{23}$$

### 2.6. *Energy resolution of multiwire proportional quantameters*

In liquid argon calorimeters with very thin sensitive layers the two reasons that make path length fluctuations not negligible in a scintillator sandwich calorimeter are no more valid. Figure 9 shows how the resolution deteriorates with decreasing argon thickness. It is clear that in multiwire proportional quantameters the resolution will be even worse than in an argon calorimeter. Very low energy electrons moving at large angles along a detector plane leave much more energy than $\theta = 0°$ electrons, also because of the larger ionization loss. This is shown in Fig. 10, which displays the results of a Monte Carlo calculation by G. Fisher and O. Ullaland. The energy deposited in some gas gaps is much larger than in others, and these high depositions are clearly due to electrons moving along the gap. Fisher has computed by Monte Carlo methods the effect of these path length fluctuations on the resolution of a gas device [15]. Some results for a lead–gas calorimeter are plotted in Fig. 11. They confirm the estimate based on eq. (21), from which we deduce that Landau fluctuations should increase the resolution by a factor $\sim 1.4$, and indicate that, in gas, path length

Table I. *Comparison between measured and computed resolutions for scintillator calorimeters*

| Ref. | Material | $t$ | $x_a$ (g cm$^{-2}$) | $E$ (GeV) | $R$(%) Exp. | $E_c$ (MeV) | $z$ eq. (5) | $F(z)^{-1/2}$ eq. (4) | $\langle\cos\theta\rangle^{-1/2}$ eq. (17) | $R$(%) eq. (18) | $R$(%) eq. (23) |
|---|---|---|---|---|---|---|---|---|---|---|---|
| 12 | Al | 1.0 | 3.0 | 10–50 | 20 | 3.0 | 0.168 | 1.16 | 1.00 | 23.0 | 61.4 |
| 23 | Fe | 0.3–1.5 | 0.65 | 0.2–2.5 | 16.9 | 0.65 | 0.068 | 1.09 | 1.03 | 16.1 | 33.7 |
| 23 | Pb | 0.3–1.5 | 1.3 | 0.2–2.5 | 12.6 | 1.3 | 0.328 | 1.21 | 1.29 | 13.2 | 13.5 |

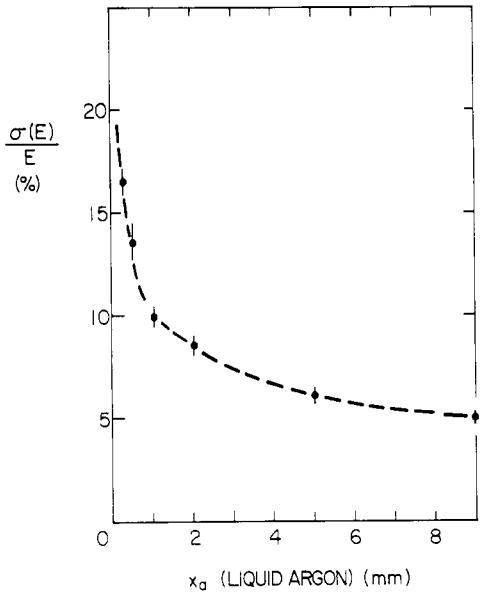


*Fig. 9.* Energy resolution vs. thickness of the active layers for 1 GeV electrons in an iron–argon calorimeter [15].

fluctuations are as important as Landau fluctuations. Combined together, these two effects multiply the sampling resolution by a factor ~ 2. This is a well known problem in the use of gas quantameters [26] and measures to cure it have been proposed. Fisher has shown [15] that the resolution can be improved by eliminating the contributions to the ionization in the gas beyond a certain distance from the shower axis (Fig. 12). This can be done either by introducing walls to stop low energy electrons (as already partially happens if one uses proportional wire tubes instead of proportional wire chambers) or by an active cut on the measured distribution of the deposited energy in the gas. This last possibility is one of the main justifications for the development of the time projection quantameter by Fisher and Ullaland and of the drift collection calorimeter by Price [25].

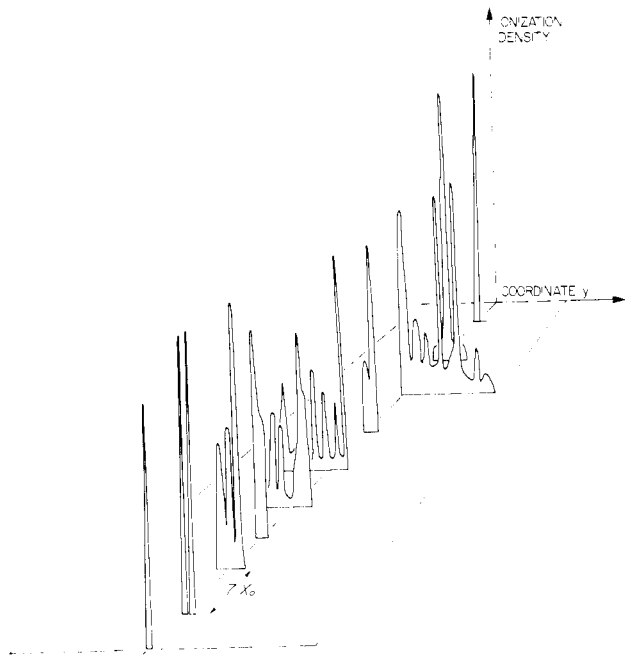


*Fig. 10.* Perspective view of the energy depositions in the gas gaps of a quantameter by a Monte Carlo generated 1 GeV electron shower. Note the large fluctuations happening, far from the shower axis, in the third and the fifth active layers.

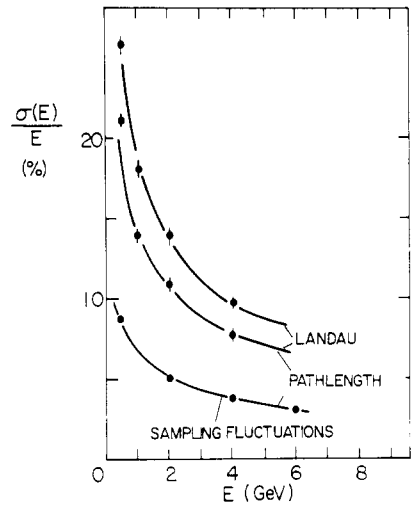


*Fig. 11.* Contributions of the sampling, path length and Landau fluctuations to the energy resolution of a lead–gas quantameter as computed by Fisher [15]. The last two effects give similar contributions (~ 12% at $E = 1$ GeV) which, combined quadratically with the sampling fluctuations (~ 7%), produce the overall resolution ~ $18\%/\sqrt{E}$.

### 2.7. *Transition effects*

Since in this paper we address the problem of fluctuations in calorimetry measurements with the aim of ascertaining the fundamental limitations, we do not treat other very important practical limitations such as photoelectron statistics, pedestal subtractions, calibration uniformity and so on. However, before closing this Section, we have to mention an important effect that occurs in sampling calorimeters and influences the absolute value of the observed deposited energy $E_{\mathrm{vis}}$. This effect is apparent when a sampling calorimeter is calibrated by using particles of known momentum (for instance muons) moving perpendicularly through the active and passive layers of thickness $x_a$ and $x_p$ respectively. If $P_a$ is the average pulse height seen in any one of the active layers, the "number of equivalent particles" in a fully contained shower producing a pulse height $P_{\mathrm{sh}}$ is

$$n_{\mathrm{eq}} = \frac{P_{\mathrm{sh}}}{P_a} \tag{24}$$

and the visible energy is

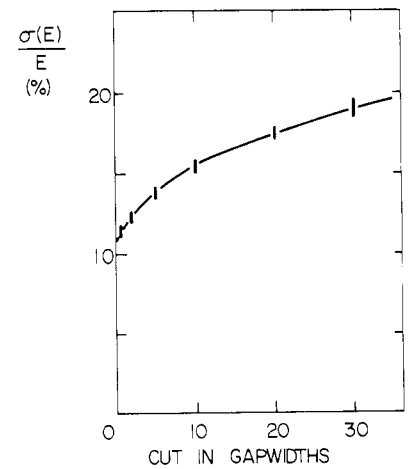


*Fig. 12.* Fisher's results on the improvement achievable by neglecting the energy deposited in the gas gaps far away from the shower axis. The distance from the axis is measured in gap widths. Multiple scattering is neglected in the Monte Carlo calculation. It introduces an effective cutoff that reduces the gain which is achievable with an external cut.

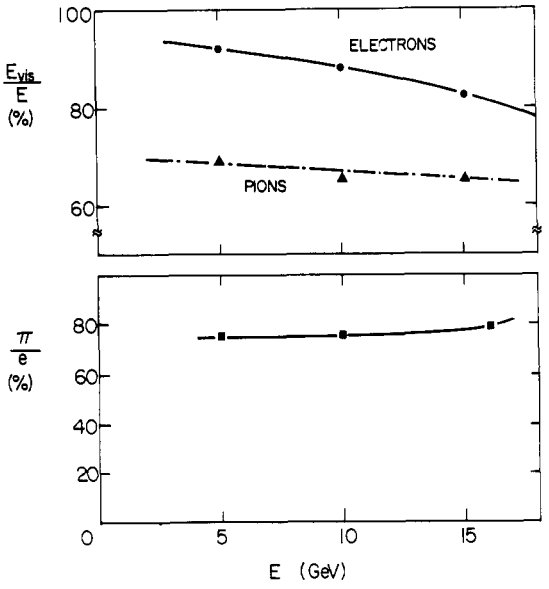


*Fig. 13.* Ratio of the visible energy to the incoming energy for electrons and pions illuminating the calorimeter of Cheshire et al. [28]. The lower part of the figure shows the energy dependence of the ratio between the pion and the electron visible energies. This ratio is ~ 0.75%. The missing 25% is spent in undetected nuclear phenomena.

$$E_{\text{vis}} = \left[\left(\frac{\Delta E}{\Delta x}\right)_a x_a + \left(\frac{\Delta E}{\Delta x}\right)_p x_p\right] n_{\text{eq}} \qquad (25)$$

where the average stopping powers have to be computed by taking into account the momentum of the particles used for the calibration. The experiments show that the ratio $E_{\text{vis}}/E$, where $E$ is the energy of the incoming electron, is always smaller than 1. For instance, Stone et al. [23] found that for a lead-scintillator calorimeter this ratio is equal to 0.52 ($x_a = 0.63\,\text{g cm}^{-2}$; $x_p = 24\,\text{g cm}^{-2}$). Cobb et al. [27] report a ratio 0.7 for a liquid argon–lead calorimeter with $x_a = 0.28\,\text{g cm}^{-2}$ and $x_p = 17\,\text{g cm}^{-2}$. For the light marble calorimeter ($x_a = 3\,\text{g cm}^{-2}$; $x_p = 23\,\text{g cm}^{-2}$) the CHARM collaboration found $E_{\text{vis}}/E \simeq 0.85$. The results obtained by Cheshire et al. [28] in a tungsten scintillator calorimeter are plotted in Fig. 13 vs. the energy of the incoming particles. Note that in this case the first 5 radiation lengths are made of fully active CsI scintillators, so that the initial part of the cascade is much better sampled than in a normal calorimeter.

These very sizeable effects are often attributed to "transition effects" in the light active material, i.e., to the abrupt increase of the electron collision losses on crossing the boundary. Indeed, at such a boundary, while the materialization rate per radiation length of the photons remains unchanged, the collision losses per radiation length (i.e., the critical energy) increases by a large factor disturbing the photon–electron equilibrium with a consequent reduction of the electron flux. Some years ago the reduction expected in Approximation B was computed by Pinkau [29]. Direct measurements have also been performed [10, 30]. They show [10] that a 0.9 cm thick acrylic layer immersed in lead reduces the electron flux by ~ 20%. This is the difference, as measured with photosensitive films ($E_c \simeq 0$), between the fluxed upstream and downstream of the acrylic layer. Such a transition effect has not to be confused with two other phenomena which also reduce the number of equivalent particles $n_{\text{eq}}$. (A) when low-$Z$ layers are interspersed in a block of heavy material the track length, which is proportional to $E/\epsilon$, decreases because the average critical energy increases. (B) due to multiple scattering, the pathlength of electrons is relatively longer in the high-$Z$ passive material than in the low-$Z$ active layers. Equation (25) takes already into account effect (A), while effect (B) contributes, together with transition effects, to make the ratio $E_{\text{vis}}/E$ smaller than 1. To our knowledge there is no detailed study of the relative contributions of these, and possibly other, effects to the response of sampling calorimeters to electromagnetic showers.

### 2.8. *Position measurements*

In this section we concentrate on the achievable accuracies in the measurement of the impact point of a gamma ray. The intrinsic resolution of such a measurement is very small, because the electron and the positron are created by the photon of energy $E$ at angles of the order of $m_e c^2 \ln (E/m_e c^2)/E$ and their multiple scattering in less than one radiation length widens the spatial distribution to a negligible amount. The limitations are thus of practical nature and have to do with the longitudinal granularity of the calorimeter and with the transverse size of its cells.

Let us first consider the case of a matrix of total absorption counters whose lateral size $d$ is comparable to the width of an electromagnetic shower. The IHEP group has built such a lead-glass detector with a size $d = 3.5$ cm and has developed an algorithm to deduce the coordinate of the impinging photon from the pulse heights observed in contiguous counters [31, 32]. The dependence of the r.m.s. value of transverse coordinate $y$ on the size $d$ of the cell is shown in Fig. 14(a) [13]. Figure 14(b) reproduces the results obtained by Amendolia et al. [33] with a similar detector: the spatial resolution improves close to the cell edges.

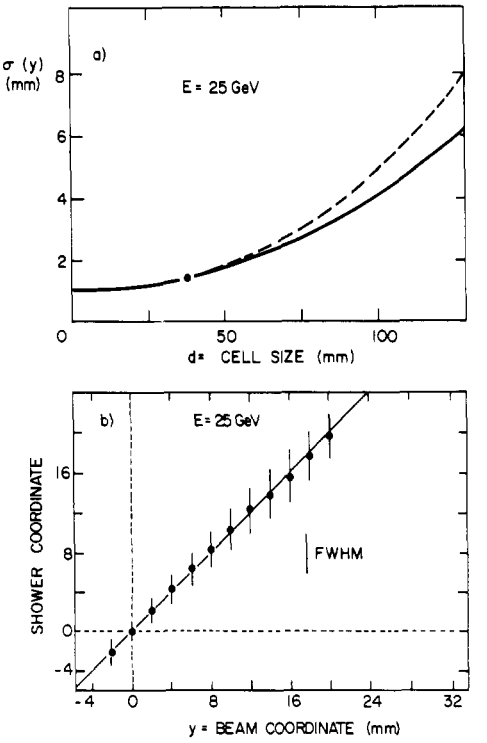


*Fig. 14.* (a) The GAMS detector of the IHEP group is made of lead glass blocks having a side $d = 3.5$ cm. The broken lines shows the $d$-dependence of the resolution for 25 GeV photons impinging at the centre of a block. The full line gives the average over block [13]. (b) Results of the Pisa group on the accuracy with which one can determine the photon position vs. the distance from the edge of the block which has $d = 3.5$ cm. The bars indicate the FWHM of the measurement [33].

Spatial resolutions of 1 mm have been obtained in these detectors around 25 GeV. Since the number of shower particles grows with the energy $E$, the scaling law should be $\sigma(y) \simeq \sigma_0/E^{1/2}$ if the lateral correlations of the number of particles are negligible. This dependence was checked in the energy range 2–40 GeV [31]. Detectors of the tower type have the added advantage of very good two-photon separation ($\simeq$ 5 cm in the above case) without suffering from the ambiguity problems typical of strip detectors. Sandwiches of lead and scintillators have also been used in the tower geometry to measure the position of a photon with a spatial resolution much smaller than the cell size [34].

In a different approach, the early part of the shower is sampled to determine its impact point. Multiwire proportional chambers offer the best spatial resolution and the results obtained compare well with expectations. The curve of Fig. 15(a) represents the predictions of a Monte Carlo simulation by Gabathuler et al. of the electromagnetic cascade with $E_c$ = 1 MeV [35]. It shows how the spatial resolution $\Delta y$ (FWHM) obtained by using the proportional information varies with the width $d$ of the detecting elements placed after 2.7 radiation lengths of lead glass. The measured points agree with the calculation. Figure 15(b) indicates that the distance between the showering block and the detector plane must be as small as possible because, due to the angular spread of the shower electrons, the resolution deteriorates quite rapidly with increasing distance. The Monte Carlo simulation shows that the achievable spatial resolution is practically unchanged when the thickness of the showering material is varied in the range 2–4 radiation lengths. In the energy range 10–50 GeV this method allows two-particle separations of about 3 cm with 5% confusion.

The above results can be scaled to different materials by expressing the transverse quantities in Molière units. Since in lead glass the Molière unit is 17 g cm$^{-2} \simeq$ 40 mm, to measure the impact point of a photon it is not worthwhile having proportional elements of width $d$ smaller than $R_M/15$. In these conditions and for energies $E \simeq 5$ GeV, one single multiwire proportional plane can give a resolution $\Delta y$ at FWHM of the order of $0.2R_M\sqrt{\epsilon}/12$, where the lead glass data ($\epsilon$ = 12 MeV) have been scaled according to the statistics of the number of tracks. For lead in bulk ($R_M$ = 16 mm) this would correspond to $d \simeq 1$ mm and $\Delta y$ (FWHM) = 2.5 mm, while for iron ($R_M$ = 18 mm) with $d \simeq 1.5$ mm one would obtain $\Delta y$ (FWHM) $\simeq$ 5 mm. Any

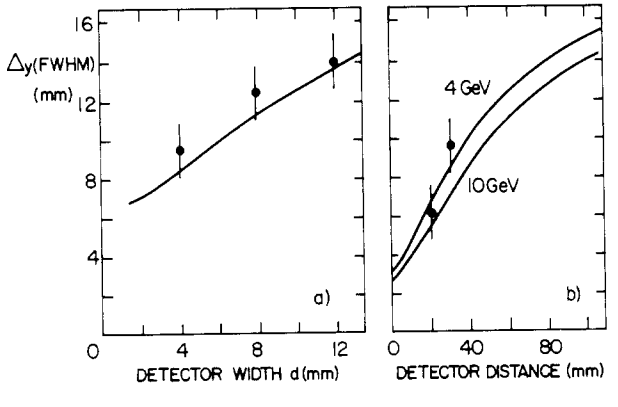


*Fig. 15.* (a) Monte Carlo predictions and data concerning the spatial resolution FWHM that can be achieved with a plane of proportional wires for 4 GeV photons [35]. (b) Effect of the distance between the showering material and the proportional wire plane for two different energies. The curves are Monte Carlo predictions.

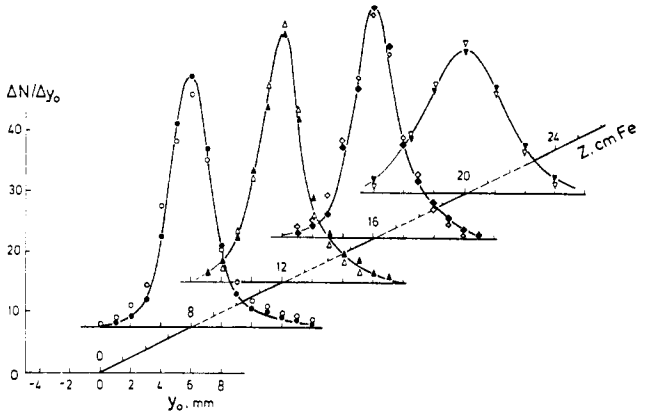


*Fig. 16.* Distribution of the centre of gravity $y_0$ of 40 GeV electromagnetic showers at different depths for two counter widths: $d$ = 5 mm (solid points) and 15 mm (empty points) [36].

decrease in average density increases proportionally the achievable spatial resolution.

Better resolutions have been obtained with scintillator strips. This should not come as a surprise, since gas proportional wires have larger fluctuations than scintillators. The IHEP group measured the resolution achievable with scintillator strips of width $d$ = 5, 10 and 15 mm immersed in lead, in lead scintillator and in iron scintillator sandwiches [36]. For large energies (20–50 GeV) the resolution does not deteriorate appreciably by going from $d$ = 5 mm to $d$ = 15 mm and in lead for $d$ = 15 mm one has $\Delta y$ (FWHM) $\simeq$ 3 mm. Figure 16 shows the distributions of shower centres of gravity $y_0$ at various depths. By comparing with the proportional wire case discussed above, we conclude that scintillator strips can be much wider than proportional wire cells and still achieve the same spatial resolution. This concept has been used by the IHEP group in the construction of an iron scintillator sandwich which measures photons with $\sigma(y) \simeq$ 2 mm at energies of many tens of GeV, but has still $\sigma(y) \simeq$ 6 mm at 0.5 GeV [37]. Two photon separations of 5 cm have also been obtained with such a detector. Argon calorimeters have reached similar spatial resolutions and separations. For instance the CELLO group [38] has obtained $\sigma(y)$ = 3 mm with 20 mm strips at $E$ = 1 GeV.

## 3. Hadronic showers

### 3.1. *General properties*

The development of hadronic showers in matter is so complicated that simplified analytical treatments are not available. However, the elementary physical processes are well understood and many Monte Carlo programs exist which simulate them. The most important properties of the interesting phenomena are summarized in Table II, which is mainly based on the presentations by Fabian, Willis and collaborators [39, 40] and by Sciulli [41].

Hadron production is insensitive to the energy and the type of the projectile and the multiplicity increases very slowly with the mass number of the target material. In pair production the photon inelasticity is 1, while the average inelasticity in a hadron interaction is one half, so that half of the energy is carried by leading particles. Neutral pions amount, on average, to 1/3 of the produced pions and their energy is dissipated in the form of electromagnetic showers. The fraction of the total energy which is dissipated in ionizations by electrons and

Table II. *Properties of the phenomena which determine the development of hadronic showers*

| Phenomenon | Properties | Influences energy resolution through | Characteristic time | Characteristic length |
|---|---|---|---|---|
| Hadron production | Multiplicity $\simeq A^{0.1} \ln s$<br>Inelasticity $\simeq \frac{1}{2}$ | $\pi^0/\pi^+$ ratio<br>Binding energy loss | $10^{-22}$ s | Abs. length $\lambda \simeq 35A^{1/3}$ g cm$^{-2}$ |
| Nuclear deexcitation | Evaporation energy $\simeq 10\%$<br>Binding energy $\simeq 10\%$<br>Fast neutrons $\simeq 40\%$<br>Fast protons $\simeq 40\%$ | Binding energy loss<br>No sampling of $n$'s<br>Poor sampling of slow parts and $\gamma$'s | $10^{-18}$–$10^{-13}$ s | Fast neturons $\simeq 100$ g cm$^{-2}$<br>Fast protons $\simeq 20$ g cm$^{-2}$ |
| Pion and muon decays | Fractional energy of $\mu$'s and $\nu$'s $\simeq \frac{5\%}{\ln E\,(\mathrm{GeV})}$ | Losses of $\nu$'s<br>Losses of $\mu$'s | $10^{-8}$–$10^{-6}$ s | $\gg \lambda$ |

charged hadrons fluctuates from event to event and is the main contribution to the energy resolution in hadron calorimetry because, while the electromagnetic energy and the energy of the charged hadrons are well sampled, a large fraction of the remaining energy is not seen. Indeed, the energy which goes either in breaking nuclei (binding energy) or in low energy neutrons is invisible; moreover many of the low energy particles (gammas and protons of few MeV) produced in the de-excitation of nuclei are badly sampled because of the short range and/or saturation effects in the active material. As pointed out by Sciulli [41] and reported in Table II, a sizeable fraction of the nuclear excitation energy goes into fast protons, i.e., protons having average energies of 150 MeV, which can be detected. Finally, muons and neutrinos emitted in the decay of pions escape detection in any reasonable size calorimeter. In a 40 GeV shower they give [39] a loss of $\sim 1\%$, which decreases with energy and will be neglected in the following.

The relative contributions of the above processes to the energy visible in a calorimeter have been determined by Monte Carlo calculations. The input formulae are by necessity approximate and the results obtained by various authors differ appreciably. This is apparent in Fig. 17, where we have summarized the results obtained by Ranft [42], Baroncelli [43] and Gabriel [44]. The first Monte Carlo was mainly devised to study shielding problems. Baroncelli's approximations are valid at high energies, while Gabriel accurately simulated the low energy and nuclear part of the cascade processes. Still, one would expect that around 10 GeV the three approaches should give consistent results, while Fig. 17 shows that the results are widely different. For instance, for 10 GeV protons the fraction of the total energy appearing in the form of electromagnetic showers is 30%, 45% and 25% respectively. (Since Baroncelli's calculation refers to positive pions, we have reduced the fraction reported in Fig. 17(b) by 10% to compare it with the other calculations.) The fractions going into nuclear binding energy plus "nuclear fragments", which are the particles produced in the phenomenon named nuclear de-excitation in Table II, appear to be 40%, 35% and 35% at 10 GeV. In this case the three calculations give similar results, all of them pointing to the well-known fact that about 1/3 of the total energy of a hadronic shower is practically invisible. The more detailed calculations by Gabriel show that 2/3 of this energy (i.e., $2/9 \simeq 20\%$ of the total) is totally lost because it is spent to compensate for the binding energy of the disrupted nuclei, while 1/3 of it (i.e., $\simeq 10\%$ of the total) goes into nuclear fragments. Table II shows that half of this energy ($\sim 5\%$ of the total) appears under the form of "fast" protons, i.e., protons of about 150 MeV. As pointed out by Sciulli [41], this energy can be sampled if the thickness of the calorimeter layer is smaller than the range of 150 MeV protons, i.e., less than $\sim 3$ cm of iron [41].

As already mentioned, shower fluctuations dominate the energy resolution of a hadron calorimeter. The average number of $\pi$'s in a shower is small and its fluctuations large. This is illustrated in Fig. 18b, which shows the 1 r.m.s. band for the total number $n_0$ of $\pi^0$'s in a shower initiated by $\pi^+$ of energy $E$ in iron [45]. It is seen that this number increases as $\ln E$,

$$n_0 \simeq 5 \ln E\,(\mathrm{GeV}) - 4.6 \quad (E > 2.5\ \mathrm{GeV}), \tag{26}$$

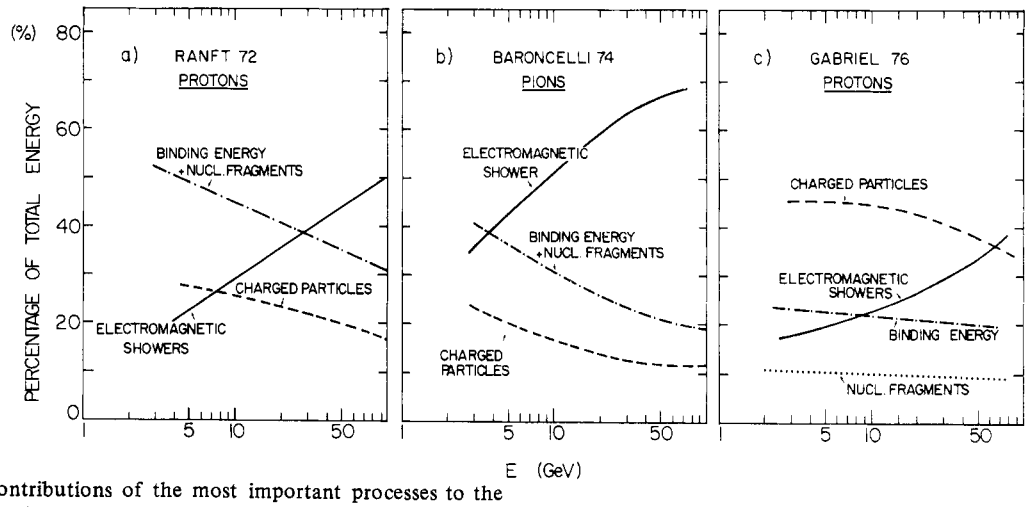


*Fig. 17.* Relative contributions of the most important processes to the energy dissipated by hadronic showers in iron. The Monte Carlo calculations are by Ranft [42], by Baroncelli [43, 45] and by Gabriel [44].

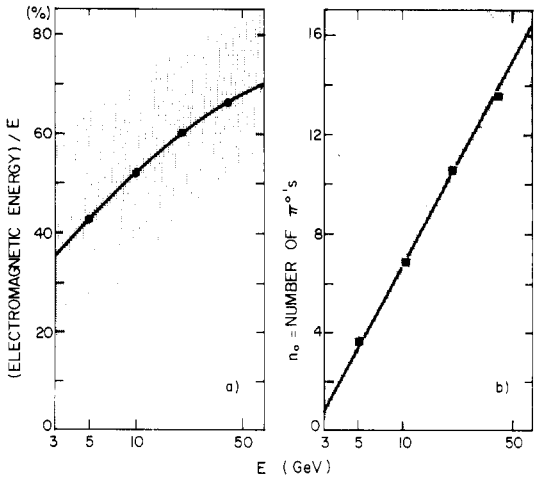


*Fig. 18.* The points are (a) the average ratio between the electromagnetic energy and the initial energy in iron and (b) the number $n_0$ of $\pi^0$'s as computed by Baroncelli [45]. The bands represent ± 1 r.m.s. around the central value.

and that the r.m.s. value of the distribution, which is reasonably symmetric around the central value, is approximately equal to $\sqrt{n_0}$. Figure 18(a) shows the ± 1 r.m.s. band for the fraction of the total energy dissipated in the form of electromagnetic showers, as computed by Baroncelli's Monte Carlo. If all the other forms of energy were invisible, the width of the band would be directly related to the achievable energy resolution. Fortunately, as seen above, about half of the remaining energy is sampled and the electromagnetic fluctuations are partially compensated by the energy dissipated by relativistic charged particles and by fast protons.

### 3.2. *Effect of containment on energy resolution*

Figure 2(a) reproduces the Monte Carlo results of Jensen, Amburgey and Gabriel [8] and illustrates the fluctuations in the longitudinal development of hadronic showers induced by pions and protons in an iron–liquid argon calorimeter. By comparing the curves drawn in Fig. 2(a) and in Fig. 2(b) one gets a visual impression of the differences between electromagnetic and hadronic showers: fluctuations multiply the average energy deposited in one plane by a factor equal to ~ 5 in the case of hadrons, while the same factor is ~ 1.5 in the case of electrons and photons.

In a hadronic shower the energy deposited in a layer of matter initially rises as a function of depth (Fig. 2(a)). In iron this rapid rise is partly due to the electromagnetic component. Beyond the maximum the energy deposition is essentially due to the hadronic component and the decrease is slow. Iwata compiled many different empirical formulae that give the median depth of hadronic showers [2] and concluded that a good representation of the data is given by

$$x_{\mathrm{med}} = [0.54 \ln [E(\mathrm{GeV})] + 0.4] \lambda_0 \tag{27}$$

where $\lambda_0$ is the nuclear absorption length. For rapid calculation one can use the approximate formula

$$\lambda_0 \simeq 35 A^{1/3} \mathrm{g\,cm^{-2}} \tag{28}$$

The longitudinal development of hadronic showers is almost energy- and particle-independent when the depth is measured in units of $x_{\mathrm{med}}$. For this reason it is possible to give a general rule to contain a fixed fraction of the total energy longitudinally [2]:

$$L(95\%) \simeq 2.5 x_{\mathrm{med}} \tag{29}$$

Note that this formula parallels eq. (9) written down for electromagnetic showers. It implies that, for an iron calorimeter that has to detect 50 GeV hadrons, $L(95\%) \simeq 1.0$ m. This is an overestimate of the thickness really needed, since the formulae reported for iron by Holder et al. [46]

$$L(95\%) \simeq [6.3 \ln [E(\mathrm{GeV})] + \text{cm Fe}$$

and by Prokhoskin [13]

$$L(95\%) \simeq [9 \ln [E(\mathrm{GeV})] + 40] \text{ cm Fe}$$

both give $L(95\%) \simeq 75$ cm.

The effect of an $f = 5\%$ loss on the hadron energy resolution can be read from the graph of Fig. 5(b), which shows that the longitudinal containment is more important than the lateral one, as for electromagnetic showers. Since 95% of the energy is contained in a cylinder having $R(95\%) \simeq \lambda_0$ [2], a good iron calorimeter must have a diameter of about 250 g cm$^{-2}$, or 35 cm for full density.

### 3.3. *Energy resolution in hadronic calorimetry*

The best known *homogeneous calorimeter* is the liquid scintillator neutrino detector described by Benvenuti et al. [47]. Its energy resolution for fully contained hadronic showers can be represented by the formula

$$\frac{\sigma(E)}{E} = 9\% + \frac{11\%}{\sqrt{E(\mathrm{GeV})}} \tag{30}$$

and the ratio $E_{\mathrm{vis}}/E$ passes from 0.75 to 0.80 when the energy of the incident pions increases from 10 to 150 GeV. The large constant term of eq. (30) indicates that the resolution is not determined by the fluctuations of elementary processes proportional in number to the energy $E$, as the sampling fluctuations considered for electromagnetic showers. A large sodium iodide was also used to measure hadron energies [48], but in this case the containment corrections were too large to give useful information on the achievable energy resolution.

*Sampling calorimeters* are widely used in detecting hadron showers. No general formula can be given to describe the achievable resolution and its dependence upon energy, material and layer thickness and one has to resort either to Monte Carlo calculations or, preferably, to experimental data. In the present case sampling fluctuations give a relatively small contribution for small enough thickness of the passive layers. This has been experimentally proven by Fabjan et al. [40] with an iron–liquid argon calorimeter having 1.5 mm thick plates by comparing the signals in interleaved active layers. In this way each event is measured twice at a distance in iron of ~ 1.2 g cm$^{-2}$ and shower fluctuations can be separated from sampling fluctuations. It was found that without sampling fluctuations the energy resolution would be reduced by less than 10%.

Figure 19 is adapted from [2] and contains a selected sample of data on the dependence of the measured energy resolution upon the thickness of passive material $x_{\mathrm{p}}$. The $x_{\mathrm{p}}$-dependence is more complicated than in the case of electromagnetic showers. For $x_{\mathrm{p}} \gtrsim 100$ g cm$^{-2} \simeq 13$ cm of Fe the electromagnetic showers are sampled every $\gtrsim 7$ radiation lengths and the resolution deteriorates linearly with $x_{\mathrm{p}}$ [49]. We find that, for $x_{\mathrm{p}} \lesssim 100$ g cm$^{-2}$, in iron the resolution behaves as

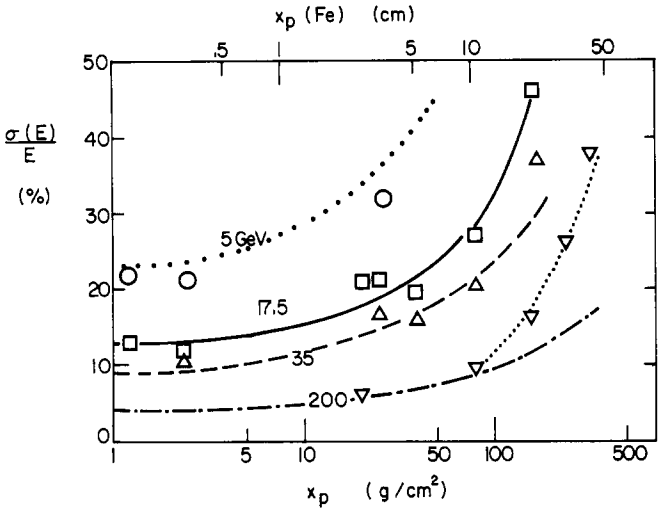


*Fig. 19.* The compilation by Iwata [2] on the thickness dependence of measured hadronic resolutions at 5, 17.5, 35 and 200 GeV is compared with the predictions of eq. (31) with $R' = 40\%$. The agreement is good below $\sim 100\,\mathrm{g\,cm^{-2}}$. The dotted curve above $100\,\mathrm{g\,cm^{-2}}$ is only meant to guide the eye through the 200 GeV points.

$$\left[\frac{\sigma(E)}{E}\right]^2 \simeq \left[\frac{50\%}{\sqrt{E\,(\mathrm{GeV})}}\right]^2 + \left[R'(\%)\sqrt{\frac{4t}{3E\,(\mathrm{GeV})}}\right]^2 \qquad (31)$$

The first term is attributed to shower fluctuations. It is sizeable because, as discussed above, about one fourth of the hadron energy $E$ is not sampled and the fluctuations on the missing 25% are very large. The second term has the typical dependence of the energy resolution for electromagnetic showers (eq. (22)) with the energy multiplied by a factor 3/4, which is approximately the fraction of the total energy dissipated in ionizations by electrons, positrons and charged hadrons. (For our present purposes there is no need to distinguish between a hadron and a lepton because, for equal energies dissipated in ionization and very low cut-off values ($E_c/\epsilon \simeq 0$), the total track length is the same.) The data collected by Iwata and presented in Fig. 19 are approximately reproduced by introducing the value $R' = 40\%$ in eq. (31). The results of the very recent measurement of the CDHS Collaboration [50] are presented in Fig. 20 together with the curves predicted by eq. (31) with $R' = 40\%$ and $R' = 30\%$. It appears that the second choice has to be preferred at low energies and for $x_p \lesssim 60\,\mathrm{g\,cm^{-2}} \simeq 8\,\mathrm{cm}$ while the first one gives an overall average fit at all energies. We shall see in Section 4.2 that, for $x_p = 2.5\,\mathrm{cm}$, the high energy data points can be brought to coincide with the low energy ones with an appropriate algorithm, so that we conclude that $R' \simeq 30\%$ gives a good representation of optimized data. For the same calorimeter eq. (18) predicts a sampling electromagnetic resolution $\sigma(E)/E = 20\%/\sqrt{E}$ in agreement [51] with the measured value $23\%/\sqrt{E}$. The measured resolution corresponds to a value $R(\mathrm{Fe}) \simeq 19\%$ for the parameter appearing in eq. (22), which is close [51] to the one measured by Stone et al. [23] and by Asano et al. [24]. By comparing hadronic and electromagnetic resolutions we conclude that in Fe

$$\frac{R'}{R} \simeq 1.5\text{–}2 \qquad (32)$$

Why is this ratio not unity? We attribute at least part of the difference to the fact that charged and neutral pions form larger angles with the shower axis than the electrons of a pure electromagnetic shower. This would introduce in $R$ a correcting factor $\langle\cos\theta\rangle^{-1/2}$ which is larger than the 1.03 given for iron by eq. (17) (see Table I). Moreover, the pion track length is insensitive to the cut-off $E_c$, at variance with the electron track, and shower fluctuations between the two types of energy depositions contribute to the $t$-dependent term in the resolution.

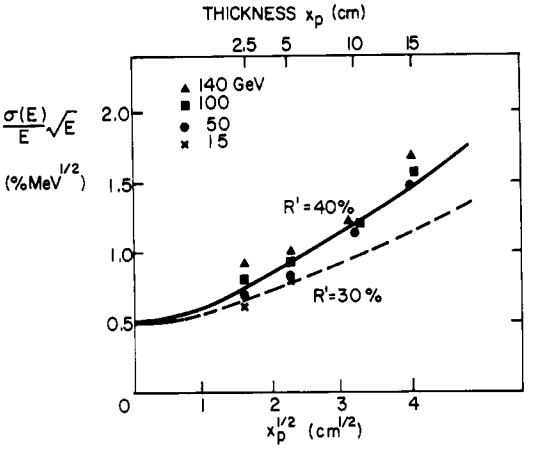


*Fig. 20.* Data of the CDHS Collaboration [50] are compared with eq. (31) for two values of the parameter $R'$.

Equation (31) shows that it is not worthwhile reducing the plate thickness below 1 radiation length, i.e., $\sim 2\,\mathrm{cm}$ of steel. In these conditions the energy resolution is dominated by shower fluctuations and is of the order of $50\%/\sqrt{E}$. One may expect that this limiting value decreases together with the invisible fraction of the total energy. Data of the CHARM Collaboration [12] seem to support such a view. In the marble calorimeter, which sees $\sim 85\%$ of the total energy, the hadronic resolution is $\sigma(E)\sqrt{E} = 53\%$, which agrees with eqs. (31) and (32) if the limiting resolution is $\sim 40\%/\sqrt{E}$. This is smaller than the $\sim 50\%/\sqrt{E}$ derived by fitting the data reported in Figs. 19 and 20 for various iron calorimeters, which typically see $\sim 75\%$ of the total energy around 10–20 GeV. However, the situation is more complicated than that, because by increasing the energy to 140 GeV, and thus increasing the fraction of visible energy to $\sim 85\%$, the CDHS Collaboration found that the resolution deteriorates with respect to the predictions of eq. (31) with a fixed value of $R'$ (see Fig. 20). In our opinion the material and

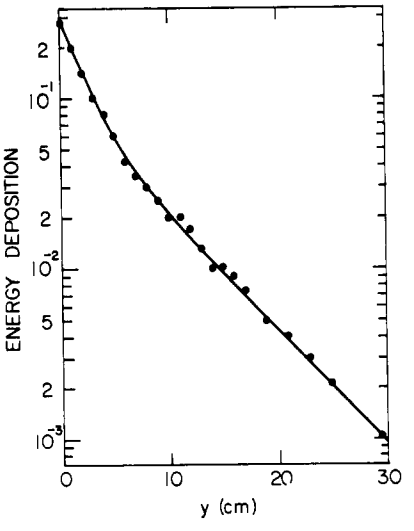


*Fig. 21.* Lateral distribution of a shower initiated by a 30 GeV antiproton in the iron calorimeter of the IHEP–IISN–LAPP group [52]. Note the two components of different slope (eq. (33)).

energy dependence of the limiting resolution is the most important open problem in hadron calorimetry.

### 3.4. *Position measurements*

Figure 21 shows the transverse distribution of a hadron shower as measured by the IHEP–IISN–LAPP Collaboration [52] with an iron-scintillator calorimeter having 5 cm wide and 1 cm thick hodoscope strips sandwiched between 2.5 cm thick steel plates. The shower can be parametrized as

$$\frac{dE}{dy} = a_1 e^{-|y|/b_1} + a_2 e^{-|y|/b_2} \tag{33}$$

with $a_1/a_2 \simeq 2$, $b_1 \simeq 2.2$ cm and $b_2 \simeq 7$ cm. It follows that accurate measurements of the conversion point of a neutral hadron (neutron, $K_0$ etc.) can be made in iron if the cells are not wider than $2b_1 \simeq 4$ cm. The Bologna group [53] measured the r.m.s. value $\sigma(y)$ at different depths in iron with 2 cm wide strips. Figure 22 shows that $\sigma(y)$ is proportional to the distance from the shower vertex in the region from ~ 15 to 55 cm, i.e., for distances larger than one interaction length. For smaller distances $\sigma(y)$ increases, probably due to albedo effects, and at the vertex is ~ 18 mm, equal at all energies. The figure shows that with a single plane of scintillator strips 2 cm wide in iron one can reach spatial resolutions which are of the order of 15 mm.

With a multilayer structure better resolutions have been achieved. Binon et al. [52] have measured the resolution in an iron calorimeter with $x_p \simeq 20\,\mathrm{g\,cm^{-2}}$ as a function of the cell size $d$. The results are shown in Fig. 23 and indicate that a reduction of the counter width from $d = 5$ to $d = 2.5$ cm does not gain very much. The dependence is of the form

$$\sigma(y) = \sigma_0(y) e^{d/d_0} \tag{34}$$

with $d_0 = 10$ cm. According to Prokoshkin [13] the energy dependence of $\sigma_0(y)$ is

$$\sigma_0(y) = \frac{15}{E}\left[\ln^4 E + \frac{E}{4}\right]^{1/2} \text{ mm} \tag{35}$$

where $E$ is, as usual, in GeV. Similar results have been obtained in the much less dense calorimeter of the CHARM Collaboration [12]. Figure 24 shows the energy dependence of the vertex determined by planes of 3 cm wide gas proportional tubes separated by marble layers 1 radiation length thick ($\simeq 25\,\mathrm{g\,cm^{-2}}$). The spatial resolution is $\sigma(y) \simeq 30$ mm at 40 GeV, worse than in an iron calorimeter with 3 cm strips because of both the lower density and the use of gas counters instead of scintillators. Finally, we remark that, for the iron calorimeter with $d = 5$ cm, Fig. 21 shows that two parallel showers overlap by ~ 1% when their vertices are separated by more than 25 cm and that the coordinates of two showers can be disentangled if they are separated by $\gtrsim 15$ cm [52].

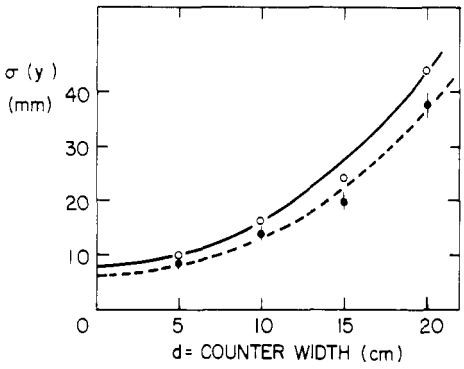


*Fig. 23.* Spatial resolution vs. strip width measured by the IHEP–IISN–LAPP Collaboration at 25 GeV (open points) and 40 GeV (solid points). The curves are fits based on eq. (34).

## 4. Methods to reduce the effects of fluctuations

### 4.1. *By software*

As an example we consider the measurement of the hadronic energy in the iron-scintillator calorimeter of the CDHS Collaboration [50]. Figure 25(a) is a scatter plot of the total energy measured, when a large number of 140 GeV pions impinges on the calorimeter, vs. the maximum energy deposited in any single counter. The observed correlation agrees with the idea that larger total energies are observed for showers that contain a larger fraction of electromagnetic energy, which in turn produces high concentrations of ionization because in iron the radiation length ($14\,\mathrm{g\,cm^{-2}}$) is much shorter than the nuclear absorption length ($140\,\mathrm{g\,cm^{-2}}$). The hadronic energy

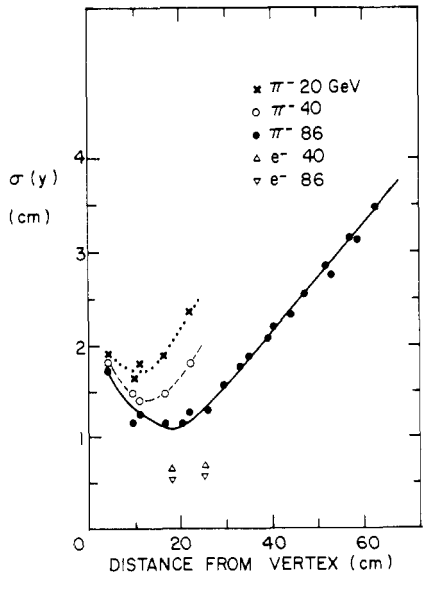


*Fig. 22.* r.m.s. value of the transverse distribution of a hadronic shower at different depths in iron as measured by the Bologna group [53].

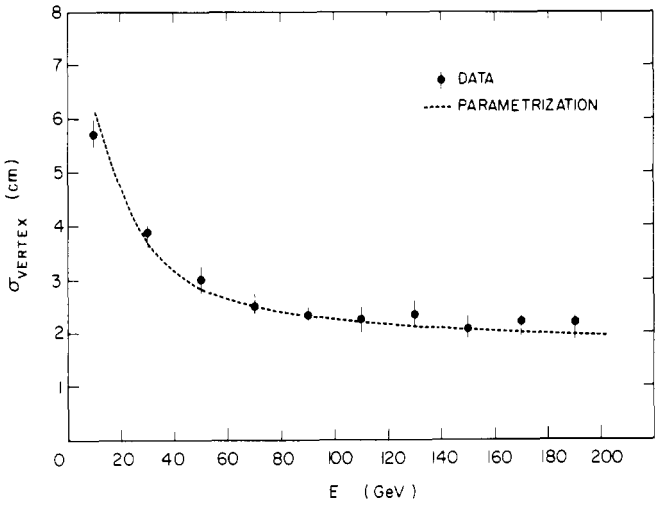


*Fig. 24.* Results of the CHARM Collaboration on the energy dependence of the spatial accuracy of the shower vertex in a light calorimeter equipped with $d = 3$ cm proportional wire tubes [12]. The parametrization is $\sigma_{\mathrm{VERTEX}} = [19.5/\sqrt{E} + 0.003E]$ cm with $E$ in GeV.

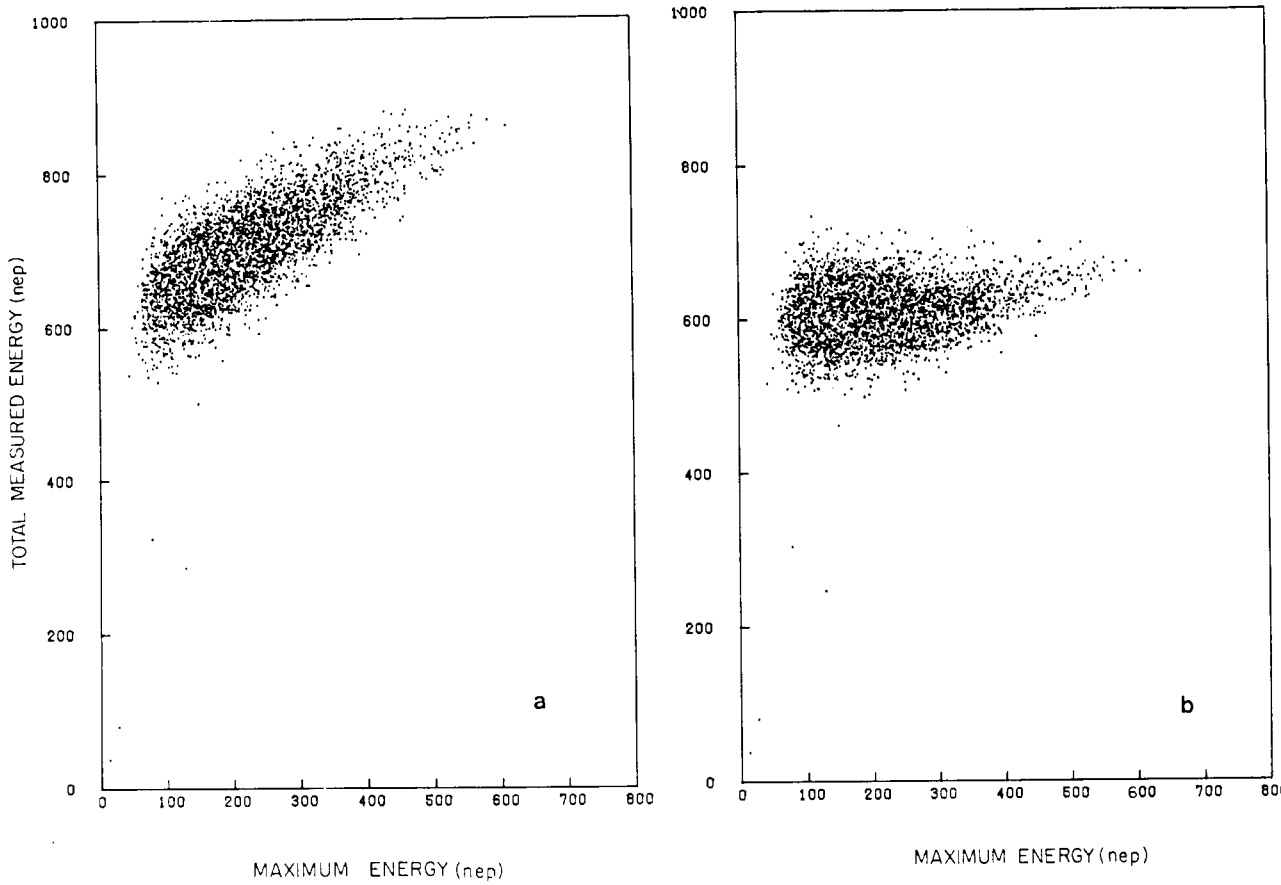


*Fig. 25.* (a) CDHS results on the correlation between the measured energy and the maximum energy deposited in any single counter for 140 GeV pions. The energy is measured in number of equivalent particles (eq. (24)). (b) Scatter plot of the same events after reducing the individual responses of the counters by a fraction proportional to the unweighted response (eq. (36)).

resolution is plotted in Fig. 26 vs. the pion energy. The open points are the results of the standard analysis, while the full ones are obtained through a weighting procedure, an idea introduced by the Caltech–Fermilab group [54]. The response $e_i$ of each counter was reduced according to the formula

$$e_i' = e_i \left(1 - \frac{C}{\sqrt{E}}\, e_i\right) \tag{36}$$

never allowing the correction factor to be smaller than 0.70.

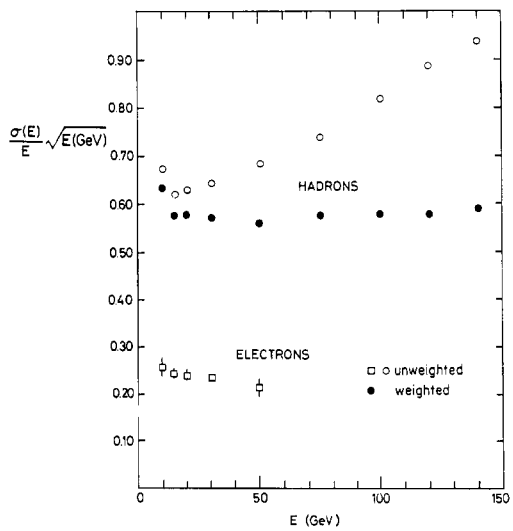


*Fig. 26.* Energy resolution of the 2.5 cm iron calorimeter of the CDHS Collaboration vs. the energy of the impinging particles. When the weighting procedure of eq. (36) is applied, the resolution improves, particularly at large energies.

The optimum value for the constant was found to be $C = 0.03 n_{eq}^{-1/2}$. This procedure reduces the correlation between $e_{max}$ and $E_{vis}$ as shown in Fig. 25(b), and produces a resolution which is well fitted by the expression $\sigma(E)/E = 0.58/\sqrt{E}$ ($E$ in GeV as usual).

This example illustrates the features of many software methods developed to reduce the effects of fluctuations: use the information content of the observed correlations and a qualitative understanding of the underlying phenomena to weight the data. Similar approaches are also adopted in spatial and angular measurements, when low weights are given to the energy deposited far away from the shower axis.

### 4.2. *By hardware*

As a first example we consider the measurement of electromagnetic energy with lead-glass counters. The low transparency of the glass for the blue part of the Cerenkov light spectrum makes the pulse height measured by a photomultiplier viewing the bottom of the block sensitive to the longitudinal shower distribution. It has been shown by the Monte Carlo calculation of Hanin and Stern [55] that, through this effect, the longitudinal fluctuations of the shower give a major contribution to the width of the pulse-height spectra. They also showed that, by excluding the wavelength shorter than 5000 Å with a light filter, the number of photoelectrons produced by a 10 GeV photon decreases by almost a factor 3, while the energy resolution passes from 7.7% (FWHM) to 5.0%. This example illustrates a general feature of the fight against fluctuations: when statistics do not dominate, even a qualitative understanding of the sources of fluctuations may suggest useful remedies.

The second example is too well known to be discussed in detail. It is the uranium hadronic calorimeter proposed by Fabjan et al. [40] to compensate the fluctuations due to the missing energy with the nuclear fissions produced by neutrons in uranium. With the argon–uranium calorimeter of [40] these authors showed that the hadron resolution is $\simeq 30\%/\sqrt{E}$, definitely superior to the resolution obtained with iron calorimeters (eq. (31)). The improve resolution goes together with an increase of the ratio between the visible energies for pions and electrons from $\pi/e \simeq 0.70$ in argon–iron to $\pi/e \simeq 1.05$ in argon–uranium. More recent experimental work [56] indicates that uranium plates 2 mm thick alternated with 2.5 mm scintillator layers give very good hadronic and electromagnetic resolutions: $32\%/\sqrt{E}$ and $14\%/\sqrt{E}$ respectively [57]. However, in this calorimeter a preliminary analysis gives a ratio $\pi/e \simeq 0.9$, still smaller than 1.

The discussions of Sections 2 and 3 suggest some possible lines of hardware development on the way to reach better energy resolutions. As far as electromagnetic showers are concerned, it seems that calorimeters with dense active layers thicker than $\sim 1\,\mathrm{g\,cm^{-2}}$ ($E_c \simeq 0.5$ MeV) are limited by sampling statistics and reach the resolution given by eq. (18). For thinner layers other sources of fluctuations play a role and the best resolutions are achieved when the detector directly counts the number of electrons traversing the gaps. This concept was tested by Conversi and collaborators by means of plastic flash tubes [18]. Since the main sources of fluctuations are the electrons moving along the gaps, Iarocci and collaborators suggested a detector based on a lattice of cubes, whose walls would stop the dangerous electrons [19]. A similar cube lattice working in Geiger mode would have some advantages and is at present under study [58]. A possibility, also mentioned by Sauli [59], is offered by the use of multistage chambers which detect the entrance point of a particle in the gap and not the total ionization deposited in the gas.

Hardware improvements in hadron calorimetry will follow from a better understanding of its limitation, and in particular of the relation between energy resolution due to shower fluctuations (which is of the order of $50\%/\sqrt{E\,(\mathrm{GeV})}$) and ratio $\pi/e$ between the visible energies produced by pions and electrons. To make this ratio closer to 1 one can think of reducing the response to electrons by constructing a calorimeter that has large transition effects, as probably already partially happens in a uranium-scintillator stack [56]. Another approach to improve the energy resolution can be based on an independent measurement of the energy going into nuclear processes. Some years ago a first attempt was made at measuring the energy going into nuclear fragments by detecting the "late" light produced by plexipop when traversed by heavily ionizing particles [60]. Other possibilities probably exist and it is hoped that this review may stimulate the reader to propose solutions to this challenging problem.

I would like to thank my colleagues of the CHARM Collaboration for many enlightening discussions on the subjects presented in this review.

## References


1. Proc. of the Calorimeter Workshop, Batavia, May 1975, M. Atac (Ed.), Fermilab (1975).
2. Iwata, S., DPNU 13-80 (May 1980). This is a part of the report for the TRISTAN ep Working Group.
3. Rossi, B., High Energy Particles, Prentice-Hall, New York (1952).
4. Nagel, H. H., Z. Physik **186**, 319 (1965).
5. Crawford, D. F. and Messel, H., Phys. Rev. **128**, 2352 (1962).
6. Longo, E. and Sestili, I., Nucl. Instr. and Methods **128**, 283 (1975).
7. A useful numerical parametrization of the shower development is given by Abshire, G. et al., Nucl. Instr. and Methods **164**, 67 (1979).
8. Jensen, T., Amburgey, J. D. and Gabriel, T. A., Nucl. Instr. and Methods **143**, 429 (1977).
9. Cerri, C. and Sergiampietri, F., Nucl. Instr. and Methods **141**, 207 (1977).
10. Yuda, T., Nucl. Instr. and Methods **73**, 301 (1969).
11. Measurements of the transverse distributions in lead-scintillator shower detectors have been recently reported, together with two component fits to the data, in Ref. [7]. See also Nelson, W. R. et al., Phys. Rev. **149**, 201 (1966) and Ref. [10].
12. Diddens, A. N. et al., CHARM Collaboration, Nucl. Instr. and Methods, **178**, 27 (1980).
13. Prokoshkin, Yu. D., Proc. of the Second ICFA Workshop on Possibilities and Limitations of Accelerators and Detectors, Les Diablerets, 4–10 October 1979, U. Amaldi (Ed.), CERN, June 1980, p. 405.
14. Hughes, E. B. et al., Stanford University Report, No. 627 (1972).
15. Fisher, G., Nucl. Instr. and Methods **156**, 81 (1978).
16. Willis, W. J. and Radeka, V., Nucl. Instr. and Methods **120**, 221 (1974).
17. Conversi, M. and Gozzini, A., Nuovo Cimento **2**, 189 (1955).
18. Federici, L. et al., Nucl. Instr. and Methods **151**, 103 (1978).
19. Battistoni, G. et al., "A cube lattice multiwire detector", Report LNF-79/12(P), 12 Feb. 1979.
20. A more detailed discussion of this effect in a gas quantameter can be found in Katsura, T. et al., Nucl. Instr. and Methods **105**, 245 (1972).
21. West, D., Proc. Phys. Soc. **A66**, 306 (1953). For recent experiments see, for instance, Onuchin, A. P. and Telnov, V. I., Nucl. Instr. and Methods **120**, 365 (1974).
22. Blunck, O. and Leisegang, S., Z. Physik **128**, 500 (1950).
23. Stone, S. L. et al., Nucl. Instr. and Methods **151**, 387 (1978).
24. Very recent and accurate data have been obtained by Asano, Y. et al. (Nucl. Instr. and Methods **174**, 357 (1980)) with a liquid argon–iron and a liquid argon–lead calorimeter. They found $R(\mathrm{Fe}) = 17.1\%$ and $R(\mathrm{Pb}) = 15.8\%$ with 2 mm of argon as active material. Equation (18) gives $R(\mathrm{Fe}) = 16.5\%$ and $R(\mathrm{Pb}) = 13\%$. While the iron data is well reproduced, the lead resolution is worse than predicted. We attribute the discrepancy to the path length fluctuations in the thin argon gap, which is more important when the angular spread of the electrons is larger (see Fig. 9).
25. Fisher, G. and Ullaland, O., Physica Scripta **23**, (1981); Price, L. E., "Drift collection calorimeters", Report ANL-HEP-CP-80-40, Physica Scripta **23**, 685 (1981).
26. For example, the lead–MWPC MAC detector has $R \simeq 24\%$ as described by Anderson, R. L. et al., IEEE Trans, Nucl. Sci., **NS-25**, 340 (1978). For further bibliography see [2].
27. Cobb, J. H. et al., Nucl. Instr. and Methods **158**, 93 (1979).
28. Cheshire, D. L. et al., Nucl. Instr. and Methods **126**, 253 (1975).
29. Pinkau, K., Phys. Rev. **139**, B1548 (1965).
30. Crannel, C. J. et al., Phys. Rev. **182**, 1435 (1969).
31. Akapdjanov, G. A. et al., Nucl. Instr. and Methods **140**, 441 (1977).
32. Binon, F. et al., Preprint IHEP 79-128, Serpukhov (1979).
33. Amendolia, S. R. et al., report Pisa 80-4 (29 May 1980), Contribution to the Conference on Experimentation at LEP, Uppsala, June 1980.
34. A resolution of $\sim 12$ mm with $10 \times 10\,\mathrm{cm^2}$ cells was obtained by Hofmann, W. et al., Nucl. Instr. and Methods **163**, 77 (1979).
35. Gabathuler, E. et al., Nucl. Instr. and Methods **157**, 47 (1978).
36. Bushnin, Yu. B. et al., Nucl. Instr. and Methods **106**, 493 (1973).
37. Buchnin, Yu. B. et al., Nucl. Instr. and Methods **120**, 391 (1974).
38. CELLO Collaboration, Contribution to the Int. Conference on Experimentation at LEP, Uppsala, June 1980.
39. Fabjan, C. W. and Willis, W. J., Ref. [1].
40. Fabjan, C. W. et al., Nucl. Instr. and Methods **141**, 61 (1977).
41. Sciulli, F. J., Ref. [1].
42. Ranft, J., Part. Accelerators **3**, 129 (1972).
43. Baroncelli, A., Nucl. Instr. and Methods **118**, 445 (1974).
44. Gabriel, T. A. and Schmidt, W., Nucl. Instr. and Methods **134**, 271

(1976).
45. Baroncelli, A., Private communication.
46. Holder, M. et al., CDHS Collaboration, Nucl. Instr. and Methods **151**, 69 (1978).
47. Benvenuti, A. et al., HPWF Collaboration, Nucl. Instr. and Methods **125**, 447 (1975).
48. Hughes, E. B. et al., Nucl. Instr. and Methods **75**, 130 (1969).
49. Barish, B. C. et al., Nucl. Instr. and Methods **130**, 49 (1975).
50. Abramowicz, H. et al., CDHS Collaboration, CERN-EP/80-188, 14 October 1980, submitted to Nucl. Instr. and Methods.
51. Note that, the scintillator thickness being only $x_a = 5$ mm, one expects a deterioration due to path length fluctuations. Figure 9 gives, for the same amount of g cm$^{-2}$, a deterioration factor ~ 1.3.
52. Binon, F. et al., IHEP–IISN–LAPP Collaboration, A hodoscope calorimeter for high energy hadrons, CERN-EP/80-15, 7 February 1980, to be published in Nucl. Instr. and Methods.
53. Bollini, D. et al., Nucl. Instr. and Methods **171**, 237 (1980).
54. Dishaw, J. P., Thesis, SLAC Report-216, March 1979.
55. Hanin, V. A. and Stern, B. E., Nucl. Instr. and Methods **157** 455 (1978).
56. Botner, O., Physica Scripta **23**, (1981).
57. It can be noted that eq. (18) gives in this case for the sampling fluctuations $R \simeq 10\%$. We attribute the difference between 14% and 10% to photoelectron statistics which, in a similar calorimeter of the same group with copper plates, contributed $\simeq 8\%$. See: Botner, O. et al., Nucl. Instr. and Methods (to be published), and CERN-EP/80-126, 14 July 1980.
58. Gygi, E. and Schneider, F., EP Int. Report 80-08, 9 Dec. 1980.
59. Sauli, F., Physica Scripta **23**, 526 (1981).
60. Amaldi, U. and Matthiae, G., Unpublished.